Ecole Centrale de Nantes

Ecole Doctorale

SPIGA

Année 2011 N° B.U. :

Thèse de Doctorat

Spécialité : Your Specilite

Présentée et soutenue publiquement par :

Your Name Here

Le 15 Novembre 2011

à l'École Centrale de Nantes

Your Thesis Title here dfsaf

Jury

Rapporteurs :	XXX XXX	Professeur, xxx
	XX XXX	Professeur, xxx
Examinateurs :	dfd fffff	Professeur, xxx
	xxx yyy	Professeur, xxx
	xxx yyy	Maître de Conférences, xxx
	xxx yyy	Professeur, xxxx
	xxx yyy	Directeur de Recherche, xxx

Directeur de thèse : xxxx xxxx N° ED
Co-encadrants : xxx xxxx
Laboratoire : xxxx en xxxxanique – Ecole Centrale de Nantes

Abstract

Add some Abstract here. and Keywords

XXXXXXXXXXXXX

XXXX

At last a three scale homogenization approach is presented for problems where the macroscale is much larger than the microscale. An intermediate mesoscale is considered, with a size lower than the RVE size. At this mesoscale comp mesoscopic modeling scale, and a spatial distribution of apparent properties coming form the previous step. Applying again classical homogenization methods at this new scale allows the determination of RVE size.

Keywords: multiscale; computational homogenization; image-based modeling; X-FEM; RVE

Résumé

The french abstract. Note the selectlanguage command in the beginning that only switch to french language in this document. Outside of this document, the language will be english.

apparentes calculées par homogénéisation sont des variables aléatoires, qui sont représentées par un développement sur le chaos polynomial identifié à partir des échantillons extraits de l'image. Des échantillons macroscopiques sont alors générés, avec une échelle de discrétisation mésoscopique, et une distribution spatiale de propriétés issue de l'approche précédente. La taille du VER est alors calculée.

Mots clés : multiéchelle ; homogénéisation numérique ; calculs sur images ; X-FEM ; VER

Contents

List of Figures

List of Tables

1. Introduction

1.1. Computational Homogenization for Multi-scale Analysis

Industrial and engineering materials, as well as natural materials are heterogeneous at a certain scale. This feature significantly influences their macroscopic behavior. In the past decades, multi-scale analysis of the mechanical behavior of multi-phase materials has been the subject of a large amount of research. A better understanding of the mechanical responses of multi-phase materials will actually advance the design and optimization of composites in industry. Multi-scale modeling is used to estimate, describe or quantify the macroscopic property of an engineering material as a function of various parameters involved at microscale. One of the key issues lies in the definition of a bridge that links different scales. Various techniques have been proposed to deal with this challenging work. Among them, a class of homogenization techniques exists and has been regarded as a powerful mean for characterizing mechanical responses of heterogeneous materials.

Homogenization technique was first developed within the framework of elasticity in order to estimate effective linear elastic properties of heterogeneous materials, see (Hill, 1963). A high level of efficiency and robustness has been reached, especially for linear properties. Some notable techniques are listed as follows

- Voigt-Reuss bounds
- Hashin-Shtrikman bounds (Hashin & Shtrikman, 1963)
- Mori-Tanaka model (Mori & Tanaka, 1973)
- Self-consistent method (Beran, 1968)

For more details see (Hill, 1963; Willis, 1981; Suquet, 1985, 1997; Nemat-Nasser *et al.* , 1998; Zohdi & Wriggers, 2005; Ostoja-Starzewski, 2006).

However, these techniques are based on approximations or analytical solutions which are only available for simple geometries. Suffering from these limitations, they are

usually restricted to certain microstructures and simple material models. For instance, in the case of a high contrast of material constants of constituents, the bounds are usually too loose to offer an effective estimation. Self-consistent method can give a reasonable prediction but only in the case of a very specific morphology of the components. In addition, micro-morphologies and physical behaviors of constituents of composites are becoming increasingly more and more complex.

In order to overcome these limitations, computational homogenization along with the development of computational methods has been proposed as a practical tool to estimate effective properties. This technique offers a good balance between general applicability on complex microstructures (e.g. complex micro-morphology) and the automated testing of different samples. Remarkable progresses has been made, see (Huet, 1990; Sab, 1992; Suquet, 1997; Michel *et al.* , 1999; Forest, 2000; Auriault *et al.* , 2009). The homogenization problem at microscale is indeed a boundary value problem which can be solved by FEM (Finite Element Method) or other appropriate numerical strategies. The boundary value problem normally corresponds to several types of boundary conditions (e.g. Dirichlet, Neumann or Periodic) from which apparent properties are derived.

1.2. Image-Based Computational Homogenization

Advances in medical and material imaging technology have made it possible to capture 3D high-resolution images of materials. There is also an increasing need to develop a numerical method that is able to incorporate a material image data into the numerical model. The FEM may be a preferred numerical strategy for computational homogenization owing to its robustness and accuracy.

However, mesh generation of FE model based on material images is usually a time-consuming task especially for complex 3D micro-geometries. The meshing process generally consists of (a) segmenting the material image into several groups of interest, (b) extracting geometrical surfaces of domains from the segmented data, and (c) building elements within these extracted boundaries. Despite already available robust algorithms, these techniques are often time-consuming and intractable for the complex topologies typical of image data. In most cases, it can not mesh multi-domains, as multiple surfaces are often non-conforming with gaps or overlaps at conjoined interfaces where manual operations are usually required.

Alternatively, the so-called *voxel-based meshing* technique can directly built a mesh from the segmented material image in an easy and straightforward way. This technique has been initially suggested by (Keyak *et al.* , 1990; Hollister & Kikuchi, 1994) and has been widely used after that. However, voxel-based mesh produces a large number of finite elements, thus leading to a huge computational cost. Practically, advanced solution techniques and supercomputers are required to solve the corresponding problem. Moreover, voxel-based meshes also produce less accurate stresses (Charras & Guldberg, 2000) due to intrinsically jagged boundaries. Although smoothing algorithms (Camacho *et al.* , 1997; Cebral & Löhner, 2001) can be employed to improve local stress accuracy, these improvements to some extent are still limited to certain applications.

In certain applications where complexities of mesh generation based on material images are issues of concern, it is appealing to develop a numerical approach which on one hand decreases meshing complexities, but still possesses a reasonable accuracy on the other. In view of that, an alternative computational approach (Moes *et al.* , 2003; Legrain *et al.* , 2010) has been recently proposed with the use of X-FEM (Belytschko *et al.* , 2003) as the numerical solution strategy for computational homogenization. One of the most appealing features of X-FEM is that mesh does not necessarily follow geometrical boundaries, which can significantly simplify the meshing process. Therefore, a regular (or structured) mesh is sufficient for X-FEM modeling. Moreover, the X-FEM can be coupled with the level-set method in order to combine capabilities of image segmentation.

The present work in Chapter 2 and 3 is an expand of (Moes *et al.* , 2003; Legrain *et al.* , 2010), and is dedicated to the image-based modeling for complex 2D and 3D heterogeneous materials. Image segmentation for *realistic* materials, and the combination of it into numerical models are presented. Chapter 3 is dedicated to the comparison between X-FEM and voxel-based FEM about the accuracy and efficiency. Several numerical examples (e.g. matrix-fiber, ceramic-metallic, cereal solid food) are considered in order to investigate their macroscopic properties with the use of X-FEM and voxel-based FEM. Moreover, the accuracy about microscopic quantities computed from the two approaches is also compared.

1.3. Edge Effects for Computational Homogenization

In some experiments but also in numerical simulations of heterogeneous materials, it is not convenient to treat large specimens, thus only small specimens are available for testing mechanical responses and obtaining apparent moduli. Yet the size of the specimen may have a strong influence on mechanical responses which are also sensitive to different kinds of boundary conditions (e.g. Dirichlet, Neumann or Periodic), which has been reported by (Huet, 1990; Hazanov & Huet, 1994; Jiang, 2002; Kanit *et al.* , 2003). In other words, three types of boundary conditions lead to quite different estimates (i.e. so-called apparent properties) of effective modulus. This difference decreases for an increasing size of specimen as shown in Fig. 1.1a. If the RVE[1] size is defined such that this difference is below a desired tolerance, it will lead to large specimens to determine effective properties. Of course, large specimens will require huge computational resources.

Although numerical efficiency can be achieved by solving the problem through parallel computations (Feyel, 2000; Kouznetsova, 2002), it is still appealing to determine effective properties with small specimens[2]. Computational homogenization approach usually requires an assumption of boundary conditions. This assumption will lead to an approximation of the solution near the edges of the microstructure, i.e. any kind of boundary conditions imposed on the microstructure will lead to

[1] RVE stands for the representative volume element.

[2] The small specimen will produce a relatively small number of degrees of freedom, thus leading to low computational cost.

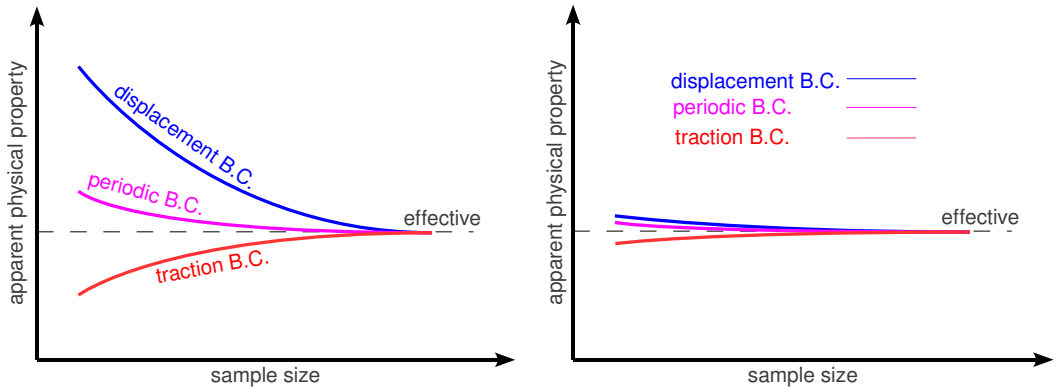

(a) Computational homogenization **(b)** Subdomain extraction approach

Figure 1.1.: Convergence of apparent properties to the effective one with increasing specimen size for different types of boundary conditions. The two figures are depicted with the same scale. In figure b, the abscissa stands for the subdomain size of a sample.

this approximation. This can be observed from the fact that different B.C.s[3] lead to difference apparent properties for a fixed specimen. **The influence caused by boundary conditions will be called *edge effects* in the following**, which can be decreased with the help of an extraction of apparent properties from an interior zone of the specimen. It involves a calculation of average strains and stresses in the interior zone, which will be called a subdomain in the following. Note that this treatment is similar to the experimental process where the loading (boundary conditions) is imposed on the specimen (sample) but only the interior region (subdomain) of the specimen is considered to obtain the physical properties (subdomain results).

The present work in Chapter 4 concerns the investigation of a subdomain extraction approach in order to obtain unbiased apparent properties from small specimens, see Fig. 1.1b. This subdomain extraction process may be viewed as a post-processing of the homogenization method. Details on the formulation of different choices of the subdomain extraction and their comparisons are illustrated. The edge effects region (i.e. boundary conditions influence region) is introduced, as well as the determination of its width. Moreover, several numerical examples are considered to investigate the accuracy of the proposed approach.

1.4. Three-scale Homogenization

In the process of computational homogenization, one needs to determine the size of the representative volume element (RVE). Mostly, the existence of a RVE is assumed and its size is initially given[4]. However, the quantification of RVE size today is still

[3]Note that here "different B.C.s" means Dirichlet, Neumann or Periodic boundary conditions. They will lead to the same results for a sufficiently large sample.

[4]In practice, the size of RVE is taken as large as possible with regard to computational resources.

a major question to be answered. Notable attempts have been made in literature (Drugan & Willis, 1996; Kanit *et al.* , 2003; Gitman *et al.* , 2007) to analyze the RVE size. The authors normally employ computational homogenization methods to test mechanical responses for increasing sample sizes and then a statistical analysis is performed to determine the RVE size.

In the statistical analysis, the key issue is to measure the mean value and standard deviation of apparent properties of concern for a series of samples with increasing volume sizes. Once the measurement of these statistical quantities is determined, various criteria combined with these statistical information can be defined to determine the RVE size in the context of different applications, see e.g. (Kanit *et al.* , 2003; Gitman *et al.* , 2007).

In the statistical process above, a series of samples with increasing volume sizes is required to be analyzed. In practice, one needs to randomly extract these samples from the whole specimen (or the whole image), i.e. so-called random subsampling or random window sampling. Moreover, the sample number required for each considered volume size is still a question to be answered.

Furthermore, the scale gap between microscale (i.e. 1μm) and macroscale (i.e. 1m) ranges from approximately $10^4 \sim 10^6$. The conventional two-scale modeling will lead to the treatment of huge data in discretization step. To overcome these limitations, a three-scale homogenization process is introduced in Chapter 5 to measure statistical quantities of concern with a low computational cost, even considering *large* macro samples. Generally, the three-scale homogenization includes the following two homogenization steps

- Step 1 From microscale to mesoscale: Computing mesoscopic properties from a two-scale modeling of micro-heterogeneities
- Step 2 From mesoscale to macroscale: These mesoscopic properties are directly used for generating macro samples on which macroscopic properties can be obtained

This is the conventional three-scale homogenization process that consists of two homogenizations. Alternatively, in this work the randomness of the mesoscopic properties is investigated and identified using the probabilistic identification. Then, this randomness is considered in the regeneration of macro samples. Owing to the separation of scales, the corresponding computational cost can be significantly decreased compared to a classical two-scale homogenization.

In order to regenerate the macro samples, a probabilistic identification of a random mesoscopic stiffness tensor is introduced with the use of polynomial chaos expansion. The coefficients of this expansion are estimated by an efficient empirical projection technique. This identification can also be used for the quantification and propagation of uncertainties of apparent properties at a certain scale.

The application of this three-scale homogenization is dedicated to the measurement of statistical quantities of concern as a function of sample size. The comparison between the proposed three-scale approach and conventional two-scale homogenization is conducted. The error propagated between scales is also analyzed for the three-scale homogenization. Finally, the RVE sizes estimated from these approaches are also presented.

1.5. Scope and Outline

The aim of this thesis is to develop an image-based computational homogenization approach with the use of X-FEM/Level-set as the numerical strategy.

In Chapter 2, the image-based modeling with X-FEM and levelset is introduced. Image-based modeling techniques are shortly reviewed. Level set image segmentation is then presented to compute the levelset corresponding to a microstructure. The X-FEM is briefly recalled, as well as various choices of enrichment functions. The combination of X-FEM and levelset is then presented. Finally, uniform and octree meshing strategies for X-FEM are mentioned with the consideration of computational cost.

In order to validate the proposed X-FEM/Levelset modeling strategy, Chapter 3 is dedicated to the comparison between X-FEM and voxel-based FEM in the framework of computational homogenization. A short review of the two approaches is introduced. Details on the formulation of microscopic boundary value problem are given. Various validation examples are also considered to investigate the accuracy of the proposed methodology and the voxel-based FEM. Chapter 3 ends with two numerical examples corresponding to *realistic* materials: a ceramic-metallic composite and cereal solid food.

In Chapter 4, a subdomain extraction method is presented with the aim of estimating the effective property from small specimens. A brief review implying edge effects (i.e. influence of boundary conditions) is first presented. Then, details on the formulation of the subdomain extraction are given. Numerical examples are finally presented to study the accuracy of the proposed subdomain approach.

Chapter 5 introduces a three-scale homogenization framework to measure some statistical quantities of interest as a function of sample volume size with a low computational cost. This chapter begins with a short introduction of available definitions of RVE. A criterion designed for tracking standard deviation of apparent properties is discussed. A probabilistic identification of random apparent stiffness tensor is introduced using polynomial chaos expansion. Thereafter, the regeneration of microstructures with the help of the identified random stiffness tensor is presented. At last, numerical examples are given to assess the accuracy of the proposed methodology versus the two-scale approach. Likewise, the estimated RVE sizes obtained from different approaches are depicted.

Chapter 6 gives a brief summary of the conclusions and recommendations in practical applications of the proposed techniques and methodologies. Perspectives of future developments of this work are shortly discussed.

2. Image-based Computational Modeling

2.1. Introduction

Recent advances in medical and material imaging technology, such as SEM, MRI, CT and UIS (Wagner *et al.* , 2007), have made it possible to characterize microstructures

$$\Gamma = \{\boldsymbol{x} \,|\Phi(\boldsymbol{x}) = 0\} \tag{2.1}$$

This chapter is be organized as follows. Image segmentation which is regarded as a prerequisite for image-based modeling, is given in §2.2. In particular, levelset image segmentation is discussed in detail. §2.3 presents the X-FEM and some enrichment functions for material interfaces, as well as the coupling of X-FEM and levelset. Finally, in §2.4 octree-based meshing strategies are addressed in order to decrease the computational cost.

2.2. Image Segmentation

Image segmentation is a challenging task and consists in extracting regions (e.g. multi-labeled images) or features (e.g. lines, circles etc.) from the offered images. This may be implemented through grouping pixels in similar features (e.g. in terms of intensity) to form a specific region, or the partition of an image. There are numerous algorithms available for image segmentation: edge detection, region growing, segm

Levelset Image Segmentation

The level set method has been used nitial guess and lock its iso-zero on the boundaries of the objects to the interpolation of the field between pixels, so that the

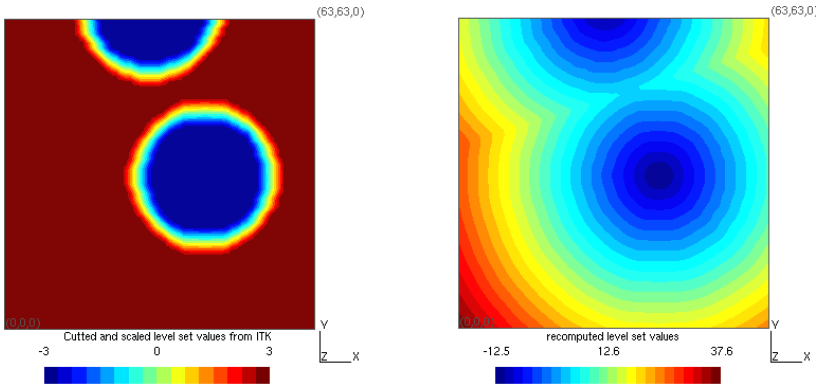

Figure 2.1.: Scaled & cut-off level set values from ITK (left) and recomputed level set values (right)

segmented geometry can be located inside the pixels. The output *level set image* where each voxel value (float type) corresponds

Tips: In ITK, taking into account the algorithm efficiency of levelset image segmentation filters, only the pixels near zero levelset in each time step are updated. As a result, levelset values calculated in the final step of segmentation do not stand for signed distances to internal material interfaces but scaled and cut-off e-consuming task. Thus, how to efficiently calculate them is also discussed in Appendix A.2.

2.3. eXtended Finite Element Method

The extended finite element method (X-FEM) (Moes *et al.* , 1999; Belytschko *et al.* , 2003) is an extension of tposed in (Melenk & Babuska, 1996). The X-FEM approximation of a field $u(\boldsymbol{x})$ takes the following form

$$u^{\text{X-FEM}}(\boldsymbol{x}) = \underbrace{\sum_{i \in I} u_i N_i(\boldsymbol{x})}_{\text{Classical}} + \underbrace{\sum_{j \in J} a_j N_j(\boldsymbol{x}) F(\boldsymbol{x})}_{\text{Enriched}} \tag{2.2}$$

whpixel-based level-set is then projected on the computational mesh, which leads to geometrical approximations, even if the element size is similar to the size of one pixel. Different strategies are discussed in the following section in order to optimize the geometrical accuracy. Finally, an illustration of the proposed workflow is presented in Fig. 2.2.

2.4. Meshing Strategies

Achievemc. Furthermore, the mesh de-refinement process enables also the use of an initial grid that is coarser than the original image (group of $n \times n$ pixels), see Fig. **??**d. Finally, note that no projection is involved during the coarsening stage,

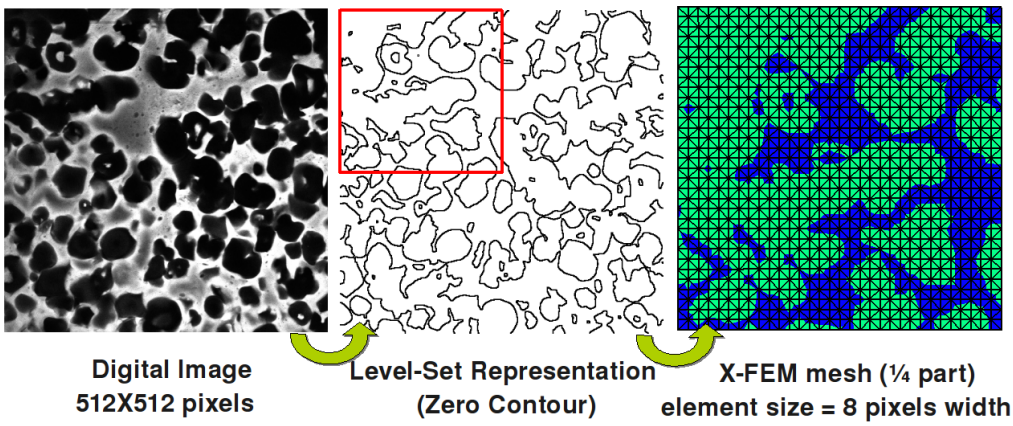

Figure 2.2.: X-FEM/levelset modeling procedure where the colors in X-FEM mesh stand for different phases divided by zero-levelset.

implying the computational efficiency of this approach. The applications of 2D and 3D Octree meshes are detailed in §3.4.2 and §3.4.3 respectively.

3. Comparison between X-FEM and Voxel-based FEM

3.1. Introduction

d X-FEM/level-set approaches. Our concern is the homogenization of two-phase composite material, focusing on micro- and macroscopic quantities of interest. Examples of fiber and particulate composite materials in elasticity are studied, their microstructure being characterized through a digital image. In this work, we also consider two realistic materials, a 2D ceramic-metallic composite material reported in (Golanski *et al.* , 1997) and a 3D foam material coming from food industry.

The X-FEM and level-set approach have been discussed in §2.3. This chapter is thus organized as follows. §3.2 is dedicated to the computational homogenization procedure. In §3.3, the proposed approach is verified through benchmark examples and compared to the voxel-based FEM. Finally, realistic examples are also considered in §3.4 and concluding remarks are given.

3.2. Computational Homogenization

In order to deal with the increasing complexity of micro-geometries and physical constitutive laws of heterogeneous materials, computational homogenization has

been proposed to estimate effective properties. Remarkable development has been made, see (Huet, 1990; Sab, 1992; Suquet, 1997; Michel *et al.* , 1999; Forest, 2000; Auriault *et al.* , 2009).

n volume element V are presented and the corresponding boundary value problems are then discussed in the following.

3.2.1. Boundary Conditions

- Periodicity conditions (PERIODIC)
- dfsddfdsf

$$\boldsymbol{u}(\boldsymbol{x}) = \boldsymbol{E}\cdot\boldsymbol{x} + \boldsymbol{u}^*(\boldsymbol{x}) \quad \forall \boldsymbol{x} \in V \tag{3.1}$$

where the fluctuation $\boldsymbol{u}^*(\boldsymbol{x})$ is periodic. It takes the same values on the opposite faces of V and the traction vector $\boldsymbol{\sigma}(\boldsymbol{x})\cdot\boldsymbol{n}(\boldsymbol{x})$ takes opposite values.

3.2.2. Boundary Value Problem

- composition

$$\begin{array}{rcccc} \langle \boldsymbol{\sigma} : \boldsymbol{\varepsilon} \rangle & \overset{\text{def}}{=} & \frac{1}{|V|}\int_V \boldsymbol{\sigma} : \boldsymbol{E}\mathrm{d}v & + & \frac{1}{|V|}\int_V \boldsymbol{\sigma} : \boldsymbol{\varepsilon}(\boldsymbol{u}^*)\mathrm{d}v \\ & = & \langle \boldsymbol{\sigma} \rangle : \boldsymbol{E} & + & \langle \boldsymbol{\sigma} : \boldsymbol{\varepsilon}(\boldsymbol{u}^*) \rangle \end{array} \tag{3.2}$$

To demonstrate Eq. (**??**) it is sufficient to prove that $\langle \boldsymbol{\sigma} : \boldsymbol{\varepsilon}(\boldsymbol{u}^*) \rangle = 0$. From Green's theorem, we have

$$\int_V \boldsymbol{\sigma} : \boldsymbol{\varepsilon}(\boldsymbol{u}^*)\mathrm{d}v = \int_{\partial V} \boldsymbol{u}^* \cdot \boldsymbol{\sigma} \cdot \boldsymbol{n}\mathrm{d}v \tag{3.3}$$

Notice that $\boldsymbol{u}^*$ takes zero values (see Eq. (**??**)) on ∂V for KUBC. In the case of PERIODIC, $\boldsymbol{t} = \boldsymbol{\sigma}\cdot\boldsymbol{n}$ bears opposite values on opposite sides of ∂V whereas $\boldsymbol{u}^*$ holds identical values (see Eq. (3.1)) on opposite sides of ∂V. Therefore, the term Eq. (3.3) vanishes and then Eq. (**??**) is verified.

- For SUBC, according to Green's theorem we have

$$\langle \boldsymbol{\sigma} : \boldsymbol{\varepsilon} \rangle \overset{\text{def}}{=} \frac{1}{|V|}\int_V \boldsymbol{\sigma} : \boldsymbol{\varepsilon}\mathrm{d}v = \frac{1}{|V|}\int_{\partial V} \boldsymbol{u}\cdot\boldsymbol{t}\mathrm{d}s \tag{3.4}$$

With Eq. (**??**), one then has ($\otimes_{\mathrm{s}}$ denotes the symmetric tensorial product)

$$\begin{array}{rcccc} \int_{\partial V} \boldsymbol{u}\cdot\boldsymbol{t}\mathrm{d}s & = & \int_{\partial V} \boldsymbol{u}\cdot\boldsymbol{\Sigma}\cdot\boldsymbol{n}\mathrm{d}s & = & \int_{\partial V} \boldsymbol{\Sigma} : (\boldsymbol{u}\otimes_{\mathrm{s}}\boldsymbol{n})\mathrm{d}s \\ & = & \boldsymbol{\Sigma} : \int_{\partial V} (\boldsymbol{u}\otimes_{\mathrm{s}}\boldsymbol{n})\mathrm{d}s & = & \boldsymbol{\Sigma} : \int_V \boldsymbol{\varepsilon}\mathrm{d}v \end{array} \tag{3.5}$$

Substituting Eq. (3.5) into Eq. (3.4), we thus have

$$\langle \boldsymbol{\sigma} : \boldsymbol{\varepsilon} \rangle = \boldsymbol{\Sigma} : \langle \boldsymbol{\varepsilon} \rangle = \langle \boldsymbol{\sigma} \rangle : \langle \boldsymbol{\varepsilon} \rangle \tag{3.6}$$

$$s_{ij}^{\text{hom}} = \left\langle \boldsymbol{\sigma}^{(i)} : \boldsymbol{\varepsilon}^{(j)} \right\rangle \overset{\text{def}}{=} \frac{1}{|V|} \int_V \boldsymbol{\sigma}^{(i)} : \boldsymbol{\varepsilon}^{(j)} \mathrm{d}v = \frac{1}{|V|} \boldsymbol{U}^{(i)\mathrm{T}} \boldsymbol{R}^{(j)} \tag{3.7}$$

It is important to notice that for a given homogenization approach, the apparent properties calculated from the direct extraction method or from energy are identical. Moreover, thanks to Eq. (**??**), the apparent stiffness tensor appears to be symmetric, which is not the case for the direct extraction.

In spite of the consideration of only the equations for 2D case, the corresponding equations for 3D case can be straightforward concluded.

3.3. Validation Examples

A homogenization problem (i.e. corresponding to a boundary value problem, see Eq. (**??**)) can be solsdfsd erning macroscopic (e.g. apparent bulk modulus and shear modulus) and microscopic (e.g. local stresses and errors) quantities.

3.3.1. Model Assessment via Effective Properties

The RVE geometry of the first sdfdsaf reference solution.

terial interface is piece-wise linear. In addition, from the image $N = 32$, the volume fraction for X-FEM is very close to the reference one ($V_f^{fiber} = 7.67\%$) while the voxel-based volume fraction converges very slowly. From the geometrical point of view, X-FEM coupling levelset is less sensitive to image resolution (mesh size) than voxel-based FEM, therefore for X-FEM one could effectively decrease the computational cost through the de-refinement of the structured mesh or octree-based mesh.

Homogenization computations using X-FEM and voxel-based FEM are conducted here to study the influence of the image resolution on the apparent properties (bulk modulus, shear modulus, defined according te of the X-FEM approach than the pixel-based one.

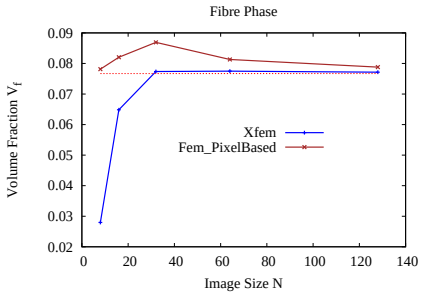

Figure 3.1.: Volume fraction V_f as a function of image resolution N

3.3.2. Model Assessment via Analysis of Local Quantities

To investigate the accuracy of X-FEM and voxel-based FEM on the microscale, a bi-material boundary w

For the sake of simplicity, a squad u^{ex} is the exact solution.

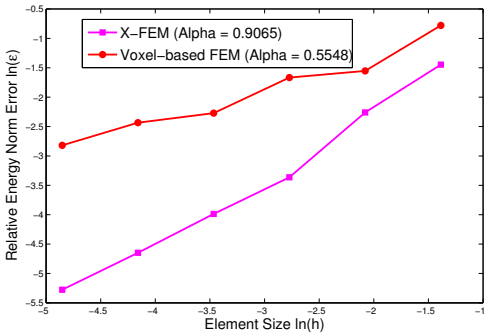

Figure 3.2.: Convergence rates with respect to the element size h

exact solution: **min=4.3088**; **max=31.4394**						
element size	Conforming FEM		X-FEM		voxel-based FEM	
$h = W/2^n$	min	max	min	max	min	max
n=3	3.83	34.9	3.31	40	3.45	24.5
n=4	3.90	33.7	2.79	33.7	1.98	32.9
n=5	3.90	33.2	3.83	32.1	1.51	35.7
n=6	3.98	32.6	3.96	32.3	2.09	37.3
n=7	4.17	32.1	4.09	31.9	1.26	39.9
n=8	**4.21**	**31.7**	**4.21**	**31.6**	**1.28**	**42.9**

Table 3.1.: Minimum and maximum σ_{11} for different approaches

In summary, this example shows that
the validation of voxel-based model must be assessed through careful considerations with regard to local quantities. Nevertheless, as for macroscopic physical properties, the voxel-based FEM might still be employed for an appropriate error.

3.4. Numerical Examples

and the voxel based FEM will also be investigated in the following.

3.4.1. A Random Fiber Reinforced Composite

The elastic as well as inelastic response of composite material is strongly influenced by its aches.

Digital Image Generation of Composite

Here a matrix-fiber composite shown in Fig. 3.3a, is randomly generated by means of in §2.2 is performed here to produce a *multi-labeled image* (input geometry of voxel-based FEM) and a *levelset image* (input geometry of X-FEM), as shown in Fig. 3.3b,c.

Numerical Results

oxel-based one, which is primarily contributed by the geometrical error Thus, the conclusion for this composite is similar as the one fiber case presented in §3.3.1.

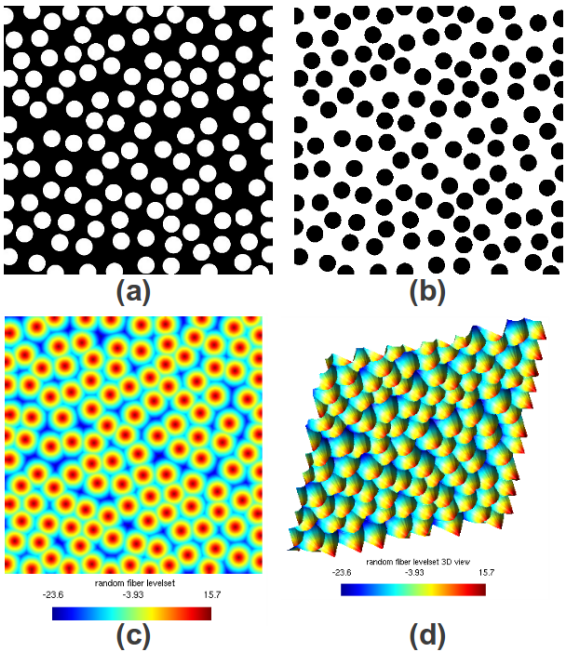

Figure 3.3.: (a) A matrix-fiber composite with randomly-distributed fibers (b) multi-labeled image as the geometry of voxel-based FEM (c) levelset value image (2D view) as the geometry of X-FEM (d) levelset value image (3D view)

3.4.2. A Ceramic-metallic Composite Material

dfsdf

3.4.3. A Real 3D Foam Material

sdfasdfsdfsdfsadfsdf

3.5. Conclusions

This chapter aimed to compare the classical voxel-based FEM to the X-FEM/level set approach proposed in (Legrain *et al.* , 2010). Voxel-based models are widely used mainly owing to the automatic mesh sdfasdfsd ut the effort of a csdfdsafsda wo approaches for 3D foam is still an issue of concern, and thus would be appealing in the future work.

4. A Subdomain Extraction Method

4.1. Introduction

sdsdfafasd

4.2. Influence of Boundary Conditions

sdfdasf

4.3. X-FEM/LevelSet for Boundary Value Problem

sadfsa

4.4. A Numerical Example

sdfsdaf

4.4.1. Determination of Sample Numbers

sdfds

Since the quantity of interest is a predefined statistical quantity of concern, one can adapt it in the context of certain applications, for example

- y may be chosen as
  - Apparent physical property, e.g. apparent bulk modulus, apparent shear modulus etc.
  - sdfdsf

4.4.2. Numerical Results

sdfsdf erval[1] is also presented. The resulting confidence interval is depicted in Fig. **??**. They all vary around the mean value ranging from 0.37 to 0.38 (cf. the *a priori* given one 37.21%), indicating the random sampling is sufficient for characterizing the geometrical property (volume fraction).

Remark 1: In order to evaluate the quality of geometries, various morphological approaches are available to test statistical features

- sdfsdfsdf
- Covariance function between two points
- Integral range (Matheron, 1971)

One may sdfsdae geometrical representativity.

Remark 2: With the use of confidence intervals, one can evaluate the quality of the estimation of the quantity of intersdfsdf redoes the estimation with another sample of size n, one might obtain a very different dispersion.

4.4.3. Apparent Physical Properties

sdfsaf the quality of obtained mean physical properties. It is clear that they all admit a small confidence interval. Accordingly, this sampling is reliable to represent the mean apparent physical property, but it does not imply the reliable representation of the variance of apparent physical properties.

Remark 1: In thisdfses, e.g. shear modulus, Young's modulus etc.

4.5. Subdomain Extraction Processing

dfd

[1] $\hat{\mu}_{\hat{\mu}_y} \pm t_{\alpha/2;n-1}\hat{\sigma}_{\hat{\mu}_y}/\sqrt{n}$, requiring an approximation by Jackknife technique.

4.5.1. Three Choices for Subdomain Extraction

sdfas

4.5.2. Comparison of Extraction Choices

all these factors, the energy-based extraction will be employed in the rest of this work.

4.5.3. Determination of Edge Effects Region

dfsf

4.5.4. Random Checkerboard

5. A Three-scale Homogenization Approach

5.1. Introduction

6. Conclusions and Perspectives

sdfsdf

Perspectives

This thesis is dedicated to the development of an enhanced computational homogenization technique. It can be used for estimating effective physical properties and the quantification of their uncertainties for multi-phase materials characterized with a huge image. In spite of a good balance between accuracy and c

- sidering covariance information among sub-units, is still a crucial issue.

Appendix

A. Calculation of Levelset Values

A.1. Calculation of Levelset Values

In the framework of X-FEM, levelset functions are used for the description of geometrical information. Th

1. tance functions. They are actually cut and scaled in consideration of algorithm efficiency. Thus, one needs to recomputed the levelset value of each node. In practice, one has

   a) In spite of the the distance to the iso-zero. This operation leads to more accurate levelset values, but bearing an expensive computational cost. In this work, the levelset values are computed from this choice.

A.2. Calculate Levelset Values of Larger Images

As reported in §2.2, the ti

- n ITK, one can calculate a rough levelset image.
- Perform levelset image segmentation employing the rough levelset image as the initial guess.

B. Jackknife Re-subsampling

In statistics, the jackknife technwhere $\hat{\theta}_j$ stands for an estimation from Y_{-j} and $\hat{\theta}_j^*$ is pseudo-value of $\hat{\theta}_j$. Accordingly, the jackknife estimator of θ can be defined as

$$\hat{\theta}^* = \frac{1}{n}\sum_{j=1}^{n}\hat{\theta}_j^* \tag{B.1}$$

Owing to the proper definition of Definition (**??**) and (**??**), one can verify that th

- distribution.

C. Random Checker Board Image Generation

In the random-field appr

1. Performing level cuts on the coarse-grained image using image thresholding. The image thresholding filter divides the whole microstructure into two phases and the threshold value determines the volume fraction of one phase.

D. Software Tools

- Image Segmentation
  - ITK
  - ITKSnap
- Image Generation: ImageJ
- Visualization
  - Paraview
  - Gmsh
- C++ Code
  - XFEM, FEM
  - Homogenization
  - Octree Meshing
- Matlab
- Comsol
- Python
- Emacs
- Lyx

Bibliography

Auriault, J.-L., Boutin, C., & Geindreau, C. 2009. *Homogenization of coupled phenomena in heterogenous media*. Vol. 1. London, UK: ISTE.

Belytschko, T., Parimi, Chandu, Moes, N., Sukumar, N, & Usui, Shuji. 2003. Structured extended finite element methods for solids defined by implicit surfaces. *International Journal for Numerical Methods in Engineering*, **56**(4), 609–635.

Beran, M.J. 1968. Statistical continuum theories. *American Journal of Physics*, **36**, 923–923.

Camacho, D.L.A., Hopper, R.H., Lin, G.M., & Myers, B.S. 1997. An improved method for finite element mesh generation of geometrically complex structures with application to the skullbase. *Journal of biomechanics*, **30**(10), 1067–1070.

Cebral, J.R., & Löhner, R. 2001. From medical images to anatomically accurate finite element grids. *International Journal for Numerical Methods in Engineering*, **51**(8), 985–1008.

Charras, G T, & Guldberg, R E. 2000. Improving the local solution accuracy of large-scale digital image-based finite element analyses. *Journal of Biomechanics*, **33**(2), 255–259.

Drugan, W J, & Willis, J R. 1996. A micromechanics-based nonlocal constitutive equation and estimates of representative volume element size for elastic composites. *Journal of the Mechanics and Physics of Solids*, **44**(4), 497–524.

Feyel, F. 2000. FE2 multiscale approach for modelling the elastoviscoplastic behaviour of long fibre SiC/Ti composite materials. *Computer Methods in Applied Mechanics and Engineering*, **183**(3-4), 309–330.

Forest, S. 2000. Cosserat modelling of size effects in the mechanical behaviour of polycrystals and multi-phase materials. *International Journal of Solids and Structures*, **37**(46-47), 7105–7126.

Gitman, I, Askes, H, & Sluys, L. 2007. Representative volume: Existence and size determination. *Engineering Fracture Mechanics*, **74**(16), 2518–2534.

Golanski, D., Terada, K., & Kikuchi, N. 1997. Macro and micro scale modeling of thermal residual stresses in metal matrix composite surface layers by the homogenization method. *Computational Mechanics*, **19**(3), 188–202.

Hashin, Z., & Shtrikman, S. 1963. A variational approach to the theory of the elastic behaviour of multiphase materials. *Journal of the Mechanics and Physics of Solids*, **11**(2), 127–140.

Hazanov, S., & Huet, C. 1994. Order relationships for boundary conditions effect in heterogeneous bodies smaller than the representative volume. *Journal of the Mechanics and Physics of Solids*, **42**(12), 1995–2011.

Hill, R. 1963. Elastic properties of reinforced solids: some theoretical principles. *Journal of the Mechanics and Physics of Solids*, **11**(5), 357–372.

Hollister, S J, & Kikuchi, N. 1994. Homogenization theory and digital imaging: A basis for studying the mechanics and design principles of bone tissue. *Biotechnology and bioengineering*, **43**(7), 586–96.

Huet, C. 1990. Application of variational concepts to size effects in elastic heterogeneous bodies. *Journal of the Mechanics and Physics of Solids*, **38**(6), 813–841.

Jiang, M. 2002. Apparent elastic and elastoplastic behavior of periodic composites. *International Journal of Solids and Structures*, **39**(1), 199–212.

Kanit, T, Forest, S, Galliet, I, Mounoury, V, & Jeulin, D. 2003. Determination of the size of the representative volume element for random composites: statistical and numerical approach. *International Journal of Solids and Structures*, **40**(13-14), 3647–3679.

Keyak, J, Meagher, J, Skinner, H, & Motejr, C. 1990. Automated three-dimensional finite element modelling of bone: a new method. *Journal of Biomedical Engineering*, **12**(5), 389–397.

Kouznetsova, V. 2002. *Computational homogenization for the multi-scale analysis of multi-phase materials*. Ph.D. thesis, Eindhoven University of Technology, Netherlands.

Legrain, G., Cartraud, P., Perreard, I., & Moes, N. 2010. An X-FEM and level set computational approach for image-based modelling: Application to homogenization. *International Journal for Numerical Methods in Engineering*, **86**(7), 915–934.

Matheron, G. 1971. *The theory of regionalized variables and its applications*. Vol. 5. Paris: Ecole national superieure des mines.

Melenk, J.M., & Babuska, I. 1996. The partition of unity finite element method: basic theory and applications. *Computer methods in applied mechanics and engineering*, **139**(1-4), 289–314.

Michel, J, Moulinec, H, & Suquet, P. 1999. Effective properties of composite materials with periodic microstructure: a computational approach. *Computer Methods in Applied Mechanics and Engineering*, **172**(1-4), 109–143.

Moes, N., Dolbow, J., & Belytschko, T. 1999. A finite element method for crack growth without remeshing. *International Journal for Numerical Methods in Engineering*, **46**(1), 131–150.

Moes, N., Cloirec, M., Cartraud, P., & Remacle, J.F. 2003. A computational approach to handle complex microstructure geometries. *Computer Methods in Applied Mechanics and Engineering*, **192**(28-30), 3163–3177.

Mori, T, & Tanaka, K. 1973. Average stress in matrix and average elastic energy of materials with misfitting inclusions. *Acta Metallurgica*, **21**(5), 571–574.

Nemat-Nasser, S, Lori, M, & Datta, S K. 1998. Micromechanics: Overall Properties of Heterogeneous Materials. *Journal of Applied Mechanics*, **63**(2), 561.

Ostoja-Starzewski, M. 2006. Material spatial randomness: From statistical to representative volume element. *Probabilistic Engineering Mechanics*, **21**(2), 112–132.

Sab, K. 1992. On the homogenization and the simulation of random materials. *European journal of mechanics. A. Solids*, **11**(5), 585–607.

Suquet, P. 1985. Elements of homogenization for inelastic solid mechanics. *Pages 193–278 of:* Sanchez-Palencia, E, & Zaoui, A (eds), *Homogenization Techniques for Composite Media*. Lecture Notes in Physics, vol. 272. Springer-Verlag.

Suquet, P. 1997. *Continuum Micromechanics*. Courses and lectures - International Centre for Mechanical Sciences. Springer.

Wagner, R.F., Metz, C.E., & Campbell, G. 2007. Assessment of medical imaging systems and computer aids: a tutorial review. *Academic radiology*, **14**(6), 723–748.

Willis, J R. 1981. Variational and related methods for the overall properties of composites. *Advances In Applied Mechanics*, **21**, 1–78.

Zohdi, Tarek, & Wriggers, Peter. 2005. *An Introduction to Computational Micromechanics*. Lecture Notes in Applied and Computational Mechanics, vol. 20. Berlin, Heidelberg: Springer Berlin Heidelberg.

Nomenclature

CT	computed tomography
ITK	Insight Tookit
MRI	magnetic resonance imaging
SEM	scanning electron microscopy
UIS	ultrasound imaging systems